# **KRAL**: **K**nowledge and **R**easoning **A**ugmented **L**earning for LLM-assisted Clinical Antimicrobial Therapy

Zhe Li<sup>a,1</sup>, Yehan Qiu<sup>b,1</sup>, Yujie Chen<sup>c,1</sup>, Xin Ding<sup>b</sup>, Yanwen Fu<sup>b</sup>, Jing Sun<sup>b</sup>, Yaguang Li<sup>a</sup>, Xinping Zhang<sup>a</sup>, Xiangyang Ye<sup>a</sup>, Jieqing Chen<sup>a</sup>, Wei Pan<sup>a</sup>, Yuna Wei<sup>a</sup>, Chao Dong<sup>a</sup>, Ziyang Huang<sup>a</sup>, Huizhen Jiang<sup>a</sup>, Lian Ma<sup>a</sup>, Dandan Ma<sup>a</sup>, Xiang Zhou<sup>a,b,\*</sup>

<sup>a</sup>Information Center, State Key Laboratory of Complex Severe and Rare Diseases,
 Peking Union Medical College Hospital, Beijing, 100730, China
 <sup>b</sup>Department of Critical Care Medicine, State Key Laboratory of Complex Severe and
 Rare Diseases, Peking Union Medical College Hospital, Peking Union Medical College
 and Chinese Academy of Medical Sciences, Beijing, 100730, China
 <sup>c</sup>Medical Intensive Care Unit, State Key Laboratory of Complex Severe and Rare
 Diseases, Peking Union Medical College Hospital, Peking Union Medical College and
 Chinese Academy of Medical Sciences, Beijing, 100730, China

# Abstract

Clinical antimicrobial therapy requires the dynamic integration of pathogen profiles, host factors, pharmacological properties of antimicrobials, and the severity of infection. This complexity imposes fundamental limitations on the applicability of Large Language Models (LLMs) in high-stakes clinical decision-making including knowledge gaps, data privacy concerns, high deployment costs, and limited reasoning capabilities. To address these challenges, we propose KRAL (Knowledge and Reasoning Augmented Learning), a low-cost, scalable, privacy-preserving paradigm that leverages teachermodel reasoning to automatically distill knowledge and reasoning trajectories via answer-to-question reverse generation, employs heuristic learning for semi-supervised data augmentation (reducing manual annotation requirements by approximately 80%), and utilizes agentic reinforcement learning to

<sup>\*</sup>Corresponding authors

Email address: zx\_pumc@163.com (Xiang Zhou)

<sup>&</sup>lt;sup>1</sup>This is the first author footnote.

jointly enhance medical knowledge and reasoning while optimizing computational and memory efficiency. A hierarchical evaluation employing diverse teacher-model proxies reduces assessment costs, while modular interface design facilitates seamless system updates. Experimental results demonstrate that KRAL significantly outperforms traditional Retrieval-Augmented Generation (RAG) and Supervised Fine-Tuning (SFT) methods. It improves knowledge question-answering capability (Accuracy@1 on the external open-source benchmark MEDQA increased by 1.8% vs. SFT and 3.6% vs. RAG) and reasoning capability (Pass@1 on the external benchmark PUMCH Antimicrobial increased by 27% vs. SFT and 27.2% vs. RAG), achieved at 20% of SFT's long-term training costs. This establishes KRAL as an effective solution for enhancing local LLMs' clinical diagnostic capabilities, enabling low-cost, high-safety deployment in complex medical decision support.

Keywords: LLM, Antimicrobial Therapy, KRAL, Agentic Reinforcement Learning, Resource-limited Healthcare

#### 1. Introduction

Antimicrobial therapy constitutes a cornerstone of modern clinical practice. The formulation of an effective regimen necessitates the integration of pathogen-specific factors, host characteristics, pharmacokinetic pharmacodynamic (PK/PD) properties of antimicrobials, and infection severity, all of which are dynamic and interrelated. This places significant cognitive load on clinicians, especially for non-infectious disease specialists or in situations where pathogens are unknown and time is limited, which may result in suboptimal prescribing decisions, thereby increasing the likelihood of therapeutic failure, antimicrobial toxicity, and the emergence of multidrug-resistant (MDR) pathogens. Large language models (LLMs) have recently emerged as promising tools for enhancing clinical decision support systems (CDSS), owing to their advanced natural language understanding and generation capabilities. Nevertheless, the direct deployment of general-purpose LLMs in high-stakes clinical domains such as antimicrobial therapy is fraught with limitations, including:

• **Knowledge bias**: Medical content constitutes <0.3 % of the pre-training corpora[1] in mainstream LLMs (e.g., GPT-3), resulting in limited coverage of rare or emerging pathogens[2–4], outdated guideline adherence[5–9](Appendix A1), and suboptimal performance on atypical presentations.

- Data privacy and compliance risks: The use of closed-source, cloud-based LLMs (e.g., GPT-4) for processing unencrypted protected health information (PHI) may violate HIPAA/GDPR-equivalent regulations, even under private deployment scenarios if online guideline updates are required [10–12].
- **High deployment costs**: Primary healthcare institutions face dual shortages of computing power and data. High-quality annotation relies on clinical experts, which consumes significant time and resources [13], particularly for medical-specific large models. Existing IT infrastructure is designed for traditional systems like HIS, lacking high-performance computing clusters for large models [14]. Upgrade costs thus represent a critical bottleneck for technological implementation [15, 16].
- Reasoning bias: LLMs are predominantly pre-trained on static, guideline-derived corpora (e.g., PubMed, MedQA), which lack real-world clinical volatility, multi-step reasoning, and patient-specific contextualization, leading to poor generalization in complex comorbid scenarios [17–19].

Among these, medical knowledge bias and reasoning bias are the most critical. Retrospective analysis of de-identified records from the open-source MIMIC-IV database and institutional EMRs at PUMCH (Appendix A2) indicates that in approximately 75% of antimicrobial prescribing scenarios, clinicians must integrate up-to-date guideline knowledge with multi-step clinical reasoning to arrive at appropriate therapeutic decisions. Consider, for example, a patient with hypertension, type 2 diabetes mellitus, chronic kidney disease (CKD), and a documented history of inappropriate antibiotic exposure who presents with community-acquired pneumonia (CAP). Selecting an "appropriate" antimicrobial regimen in this context requires:

- Comorbidity-adjusted prescribing: CKD may contraindicate renally cleared agents (e.g., aminoglycosides), whereas diabetes may modulate infection severity and wound-healing capacity.
- Resistance-risk assessment: Prior antibiotic misuse increases the probability of colonization with multidrug-resistant (MDR) organisms (e.g., ESBL-producing Enterobacteriaceae, MRSA), rendering standard first-line agents ineffective.
- **Drug-drug interaction screening**: Chronic medications (e.g., antihypertensives, hypoglycaemics) must be reviewed to avoid clinically significant interactions with newly prescribed antibiotics.

Effective management of such complex clinical scenarios necessitates LLMs capable of multi-step, context-aware reasoning and real-time access to evolving clinical guidelines. Conventional RAG frameworks do not mitigate reasoning deficits, whereas SFT demands extensive, expert-level annotation and still falls short in complex, multi-step reasoning. To address these limitations, we propose KRAL (Knowledge and Reasoning Augmented Learning), a modular, cost-efficient training paradigm that jointly enhances domain knowledge and clinical reasoning in LLMs. KRAL aims to improve the reliability, safety, and clinical utility of AI-driven antimicrobial recommendations, while remaining deployable in resource-constrained settings.

## 2. Methods

#### 2.1. Datasets

The KRAL training corpus was assembled from three institutional sources: (i) PUMCH antimicrobial guidelines, (ii) antimicrobial Q&A pairs extracted from the hospital CDSS, and (iii) de-identified electronic medical records (EMRs). The guidelines comprise 750 pages of clinician-curated PDF/JPG files covering indications, dosing, renal adjustments, and resistance patterns. The CDSS subset contains 105 manually verified Q&A pairs generated during real-world clinical consultations and subsequently validated by infectiousdisease specialists. Additionally, patient EMR data underwent inclusion & exclusion screening (Appendix A3), using medical record covers, basic information, and laboratory/imaging data as context with final antimicrobial choices serving as ground-truth labels, which was approved by the National Health Commission of China, and a waiver of informed consent was received from the Ethics Committee of Peking Union Medical College Hospital (PUMCH, ethics number I-23PJ1416). This yielded 710 de-identified cases for clinical-reasoning training; all PHI was removed under an IRB-approved protocol. To evaluate the generalization capability of the KRAL learning paradigm, two external evaluation datasets unrelated to the training data were utilized: MedQA and the PUMCH Antimicrobial Benchmark. These were applied to assess knowledge-enhanced learning and reasoning-enhanced learning effectiveness, respectively. MedQA is a publicly available online dataset compiled from professional medical board examinations. It contains questions in three languages: English (12,723 questions), Simplified Chinese (34,251 questions), and Traditional Chinese (14,123 questions). Each data entry comprises three columns: Question, Options, and Evidence. A sample dataset is provided in Appendix C3. An antimicrobial-focused subset was selected from the English-language MedQA comprising four categories: Antifungal Drugs, Antifungal Medications, Antiviral Drugs, and Antiviral Medications as shown in Fig. 10 (total n=56). The in-house PUMCH Antimicrobial Benchmark is an expert-curated, de-identified test set sampled from prospectively collected EMRs; no overlap with training data. It is divided by complexity level into three scenarios: prophylactic antibiotic therapy, routine antibiotic therapy, and complex antimicrobial therapy for drug-resistant bacteria (total n=26). Data examples are provided in Appendix C3.

#### 2.2. KRAL Pipeline Overview

The KRAL framework performs automated, multi-round knowledge-and-reasoning distillation. Each round takes (i) the current training corpus and (ii) a frozen teacher model as inputs, and outputs an updated student check-point. After a cycle, updating the knowledge base or swapping in a stronger teacher entails only uploading new documents and editing a YAML config; all downstream steps are fully automated. The remaining processes automatically rerun to regenerate the model checkpoint end-to-end. Utilizing an adapter-based approach to updating model parameters enables flexible combination of prior training results as plugins. These can be incorporated into the base model weights for specific clinical reasoning scenarios.

The single-round learning process comprises three stages as shown in Figure 1: Data Distillation, Agentic Reinforcement Learning, and Multi-expert Hierarchical Evaluation.

#### 2.3. Stage 1: Data Distillation

In this stage, a small subset of real clinical data serves as a seed database. We leverage DeepSeek-R1 (671 B) to distill structured guideline knowledge and multi-step clinical reasoning chains into a lightweight student architecture. This stage yields high-quality, task-specific corpora suitable for parameter-efficient fine-tuning of resource-constrained student models.

First, PUMCH clinical guidelines are processed through OCR structuring, document segmentation, and vectorization to form a vector database. Vectorization employs the open-source embedding model BGE-m3, which boasts robust versatility, multilingual support, and multi-granularity processing capabilities. This model offers broad application prospects in information retrieval and natural language processing. The resulting vectors are then indexed and optimized using the FAISS vector database. A caching

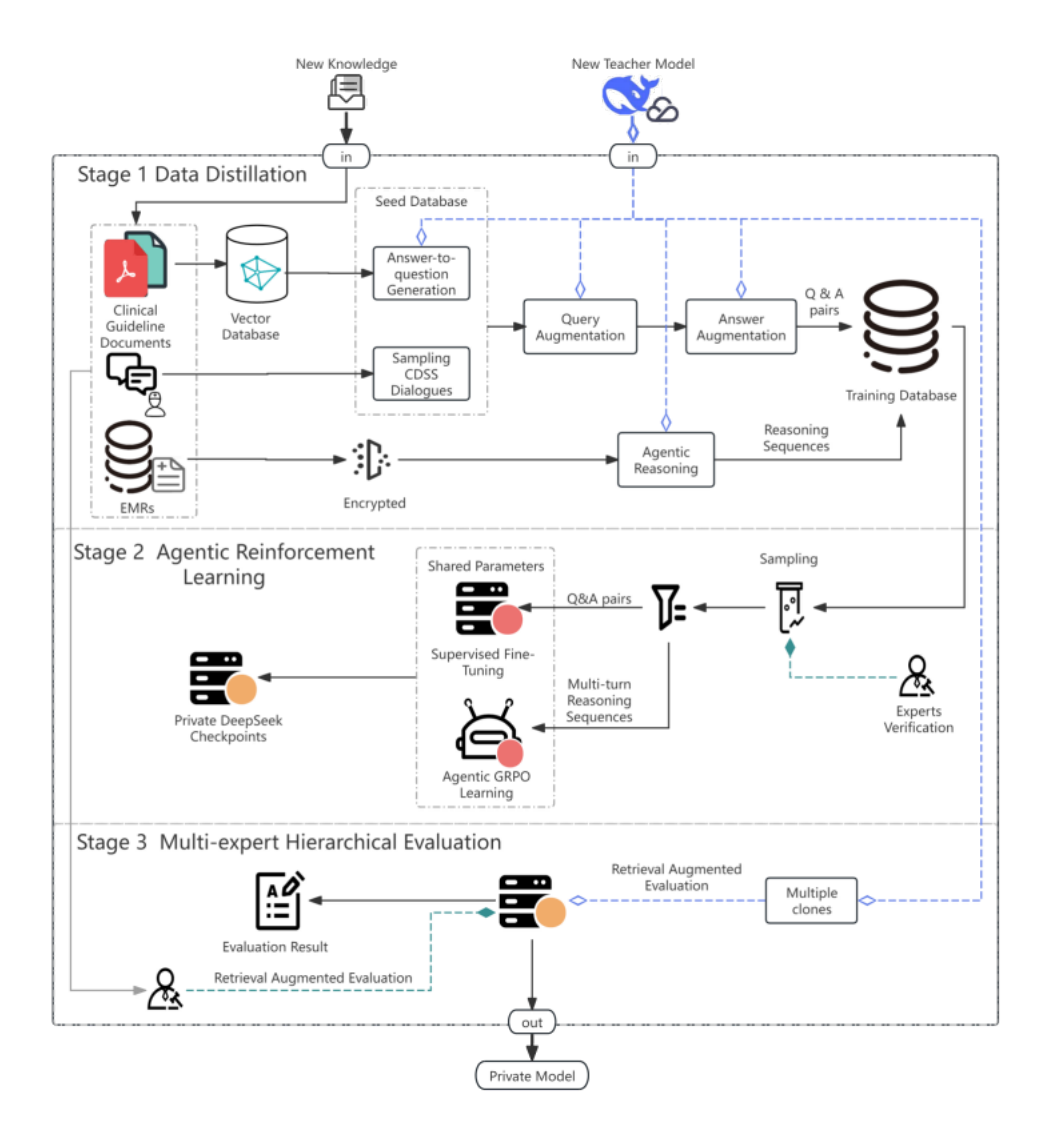


Figure 1: Overview of the KRAL paradigm

mechanism stores up to 1,000 recent search results to enhance retrieval efficiency for repeated queries. Additionally, search results are reordered using a hit-heat and timestamp-weighted sorting algorithm to optimize ranking. The full re-rank weight is computed as in follow equation:

$$R_{rank} = w_s r_s + w_p r_p + w_t r_t$$

Where the symbol  $w_s$  represents the cosine-similarity weight,  $w_p$  the evidence-frequency weight,  $w_t$  the temporal-recency weight, and  $r_{s,p,t}$  the corresponding scores.

For each retrieval, when a knowledge chunk is matched, its hit count is updated in the vector database's metadata according to the following rule, where  $\beta$  is the hit count update coefficient. Hybrid retrieval significantly improves recall accuracy (see NIH Test).

$$r_p = \text{clip}(r_p + \beta R_{rank}, 1)$$

To construct the Seed Database, we leverage LLM prompt engineering to generate Q&A data pairs in the answer-to-question manner with input knowledge chunks randomly sampled from the vector database. Additionally, 105 curated antimicrobial Q&A data points from the CDSS system are incorporated. The detailed workflow is illustrated in Figure 2. All data in the Seed Database undergoes heuristic learning through few-shot prompting to achieve 5 times query augmentation. Finally, by configuring high LLM reasoning diversity, the Teacher Model generates multiple reasoning outputs for each query using RAG, yielding 10,138 Q&A pairs stored in the training dataset. Sample data is provided in Appendix B1.

Second, to further enhance clinical reasoning, we adopt ReAct (Reasoning + Acting) to produce traceable, multi-step reasoning trajectories from teacher outputs. By specifying multi-round "Reasoning-Action-Observation" paths, it upgrades single-step outputs into verifiable, interactive, and error-correctable multi-step chain-of-thought (CoT) reasoning, significantly boosting the model's reasoning ability [20]. Figure 3 illustrates this workflow. The agent's operational steps—each action or thought—along with the final output constitute Reasoning Trajectory Data. Unlike standard SFT training data containing only query-answer pairs, reasoning trajectory data incorporates the reasoning process, enhancing stability in subsequent transfer learning. Trajectory data examples are provided in Appendix B2.

#### 2.4. Stage 2: Agentic Reinforcement Learning

The widespread application of the DeepSeek-R1 model demonstrates reinforcement learning's significant enhancement of reasoning capabilities [21]. To simulate the multi-step decision-making characteristic of clinical diagnosis while better suppressing hallucinations of critical information (e.g., medication dosage) under limited SFT training data, we employ an Agentic Reinforcement Learning approach in which agent interacts with a retrieval tool

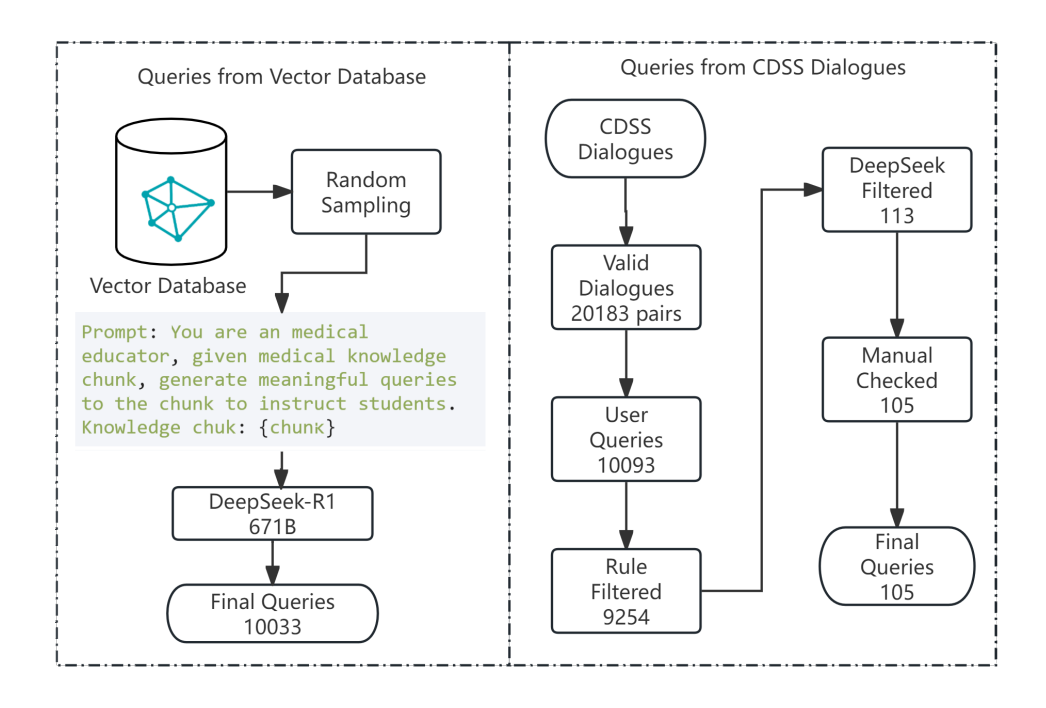


Figure 2: Schematic of the data screening procedure

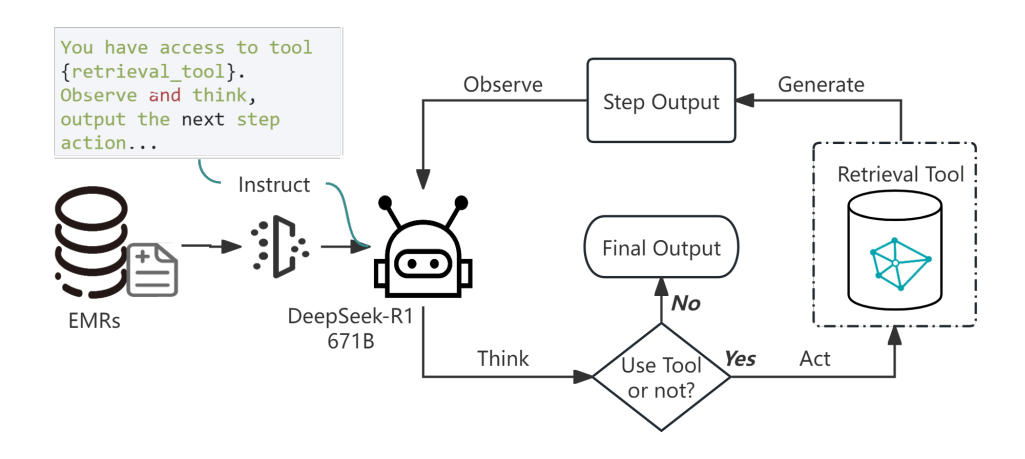


Figure 3: Reasoning trajectory distillation

and optimises a multi-turn policy via Group Relative Policy Optimisation

(GRPO). This enables online interaction between the LLM and retrieval tools during training, with the Reward Model evaluating different actions using distinct scoring logics. To address the cold start problem in knowledge transferring [22], RL requires prior supervised fine-tuning based on Q&A pairs. The training dataset comprises 30K entries, each consisting of input (patient age, gender, chief complaint, medical history, and present illness) and ground truth (actual clinical recommendations). The test set constitutes 10% of the data, with examples provided in Appendix C1. Training parameters are detailed in Table 1.

Referring to DeepSeek-R1's implementation, we employs GRPO as the reinforcement learning algorithm. Unlike PPO, GRPO eliminates the value model by normalising rewards within a sampled group, cutting GPU memory by 50 %. This significantly reduces hardware resource consumption during RL training, making GRPO more suitable for scenarios with limited hardware resources and sparse rewards in large models. Agentic GRPO was executed on 1517 clinician-verified reasoning trajectories; hyper-parameters are listed in Table 2.

Table 1: SFT Training Hyperparameters

Key	Value	Key	Value
Learning rate	4e-5	Optimizer	Adamw
Batch size	8	Gradient clipping	0.3
Training epochs	2000	Pipeline parallelism	8
Adapter type	LoRA/rank 32	Warm-up ratio	0.05
Gradient accumulation steps	4	Deepspeed type	Zero3+offload

## 2.4.1. Hardware-Efficient Implementation

Although GRPO already lowers memory, we further reduce computing cost via LoRA (rank 16), FP8 mixed precision, ZeRO-3 sharding, CPU offloading and so on.

• LoRA (Low-rank Adaptation): A parameter-efficient fine-tuning method that trains only a small portion of the model's parameters (specifically,

Table 2: GRPO training hyperparameters

Key	Value	Key	Value
Learning rate	2e-6	Optimizer	Adamw
Batch size	8	Gradient clipping	0.3
Training epochs	10	Pipeline parallelism	4
Adapter type	LoRA/rank 16	Warm-up ratio	0.1
Reward functions	Custom reward functions	Reward weights	[1.0, 0.8]
Advantage clip ratio	-0.1/+0.4	KL punishment weight	0.001

low-rank matrices) instead of the entire model, typically targeting just 0.1%-1% of parameters. When training only 1% of parameters, the computational load for backward propagation gradients is reduced by approximately 99% (theoretically reducing FLOPs proportionally). However, the computational load for forward propagation remains largely unchanged, as the base model is frozen with only minimal additional computation from LoRA. Overall, computation is reduced by about 75%, and memory usage is reduced by about 67% [23].

- FP8 mixed precision: FP8 mixed precision involves storing weights, gradients, and activations using 8-bit floating-point numbers (FP8), while employing higher precision (e.g., FP16/FP32) for critical operations. Compared to FP16, this approach reduces GPU memory usage by approximately 50%.
- Zero3[24]: Partitions optimizer states, gradients, and parameters across multiple GPUs to eliminate redundancy. Each GPU stores only its own slice, reducing memory usage in proportion to the number of GPUs (N).
- CPU offloading[25]: Offloading optimizer state, gradients, or parameters to CPU memory or NVMe storage thereby frees up GPU memory. With sufficient CPU memory, this can reduce GPU memory usage by approximately 87.5%.
- Compressed Reward Model: The number of models used for learning is reduced from two (Policy model + Value model) to one (Policy model), resulting in a 50% reduction in computational resource consumption. If GRPO's reward model employs a lightweight model such as BGE-

m3 (0.6B), GPU memory usage decreases from four models to two, achieving a 50% reduction in GPU memory consumption.

## 2.4.2. Reasoning Augmented Implementation

To further augment reasoning capabilities, the following improvements were implemented:

- 1. Asymmetric Clipping with Higher Upper Bound: The original symmetric range  $[1 \epsilon, 1 + \epsilon]$  is replaced with two hyper parameters  $\epsilon_{low}$  and  $\epsilon_{high}$ . The upper bound is relaxed to 0.28 or higher, while the lower bound remains constrained between 0.1 and 0.2. This allows model to learn 'key tokens'—those with low probability but high advantage—efficiently.
- 2. **Reward Smoothing**: A custom attention-weighted reward function incorporating medical knowledge was developed. This smoothing mechanism filters out noisy contributions in model outputs, enhancing training stability and consistently improving reasoning capabilities.

# 2.4.3. Trajectory Data Preprocessing

Prior to GRPO training, trajectory data underwent targeted preprocessing to enhance model robustness and learning efficiency. Specifically: First, prompt influence was minimized to prevent excessive reliance on context during reinforcement learning. Second, chat template adjustments preserved internal "thinking" tokens, making the reasoning process observable and learnable. Third, we reuse the teacher model with prompts to compress retrieved knowledge, eliminating irrelevant information and reducing context length. Finally, we streamlined multi-turn dialogues, retaining only the most concise effective reasoning paths. These steps focused on refining two core capabilities: (A) concise yet comprehensive analysis of medical records and conditions; and (B) rational decision-making regarding when and how to retrieve external knowledge.

#### 2.4.4. Custom EMR-aware Reward

To align the reward signal with patient's EMR data, we designed a custom reward.

1. **Progress Reward**: Given a patient's record, the model must determine whether to perform a Retrieval Action and what keywords to pass as search terms before making the final answer. An action sample is:

<action>keyword A, keyword B, keyword C... </action>. To enhance evaluation robustness, Subword-level Jaccard similarity (rather than traditional word set Jaccard[26]) is used to capture subword overlap, e.g., between 'COVID' and 'COVID-19'. Additionally, a max operator ensures each predicted term matches only the most similar ground truth term, avoiding redundant penalties. Finally, the average similarity across all predicted terms produces the final reward for the corresponding action.

2. **Subword-level Jaccard**: For any two words  $w_i$  and  $w_j$ , the subword-level Jaccard similarity is defined as:

$$\operatorname{Jaccard}(w_i, w_j) = \frac{|C(w_i) \cap C(w_j)|}{|C(w_i) \cup C(w_j)|}$$

where C(w) represents the deduplicated subword set of w. When use GT as collections of ground truth label g, P as collections of prediction p, the final similarity (i.e., Reward) can be written as:

ActionReward = 
$$\frac{1}{|P|} \sum_{p \in P} \max_{g \in GT} \text{Jaccard}(p, g)$$

3. **Hybrid Similarity**: The final reward is defined as the similarity between the predicted and ground truth textual outputs. To enhance robustness, we adopt a Hybrid Similarity metric based on embedding vector distance. This approach builds upon direct textual embedding comparisons by incorporating sparse bag-of-words similarity (lexical matching score [27]) and semantic similarity (Colbert score [28]), thereby better capturing key term and semantic similarities.

$$\operatorname{Hybrid}(P,T) = \frac{1}{N} \sum_{i=1}^{N} \max_{j} \left( \alpha S_d^{(i,j)} + \beta S_l^{(i,j)} + \gamma S_c^{(i,j)} \right)$$

Subscripts d, l, c denote dense vector distance, lexical matching score, and Col-BERT score respectively. i, j represent the chunk indices of the prediction and ground truth respectively.

4. **Repetition Penalty**: To prevent reward hacking that degrades model performance, a repetition penalty is introduced. To accommodate Chinese grammatical peculiarities, Chinese part-of-speech tagging is incorporated, preventing erroneous expressions caused by repeated text fragments with identical semantics.

5. **Hybrid Similarity Reward** The final therapy-level reward quantifies the semantic overlap between the generated regimen P and the clinician-verified reference T. We define a chunk-wise hybrid similarity:

$$\mathcal{R}_{\text{hybrid}}(P, T) = \frac{1}{|P|} \sum_{i=1}^{|P|} \max_{j \in [1, |T|]} \left( \underbrace{\alpha \cdot S_{\text{d}}^{(i,j)}}_{\text{dense cosine}} + \underbrace{\beta \cdot S_{\text{l}}^{(i,j)}}_{\text{lexical overlap}} + \underbrace{\gamma \cdot S_{\text{c}}^{(i,j)}}_{\text{ColBERT}} \right)$$

where  $\alpha + \beta + \gamma = 1$ ,  $S_{\rm d}^{(i,j)} = \cos(\mathbf{h}_p^{(i)}, \mathbf{h}_t^{(j)})$  is the dense embedding cosine;  $S_{\rm l}^{(i,j)}$  is the sparse lexical match computed with BM25 + unigram overlap [27];  $S_{\rm c}^{(i,j)}$  is the late-interaction ColBERT score [28] using medical-domain fine-tuned checkpoints. Chunks are sentence-level to preserve dose-and-schedule boundaries.

6. **Repetition Penalty.** To discourage surface-form reward hacking (e.g., repeated drug names or dosages), we penalise semantic-level duplicates:

$$\mathcal{R}_{\text{rep}} = -\lambda \sum_{k=1}^{K} \mathbb{1} \left[ \cos(\mathbf{h}_k, \mathbf{h}_{k-1}) > \tau \right] \cdot \text{POS-weight}(k),$$

where  $\mathbb{M}[\cdot]$  is the indicator function,  $\tau = 0.92$ , and POS-weight downweights Chinese function-word repetitions (POS tagged by LAC v2.1) while preserving therapeutic-content repeats (e.g., "q8h" appearing twice for dual therapy is not penalised). The final token-level reward is

$$\mathcal{R}_{\mathrm{token}} = \mathcal{R}_{\mathrm{hybrid}} + \mathcal{R}_{\mathrm{rep}}.$$

2.5. Stage 3: Multi-expert Hierarchical Evaluation

Considering clinical implementation constraints, validation data primarily consists of de-identified, unstructured medical records and treatment plans (sample data in Appendix C2). But traditional rule-based metrics (BLEU, ROUGE) show weak correlation with clinical appropriateness and full human review is cost-prohibitive (approximate USD 200 per 100 cases). We therefore implement a two-tier hierarchical evaluation protocol (Figure 4):

1. **LLMs Pre-review**: By configuring temperature-scaled autoregression and role-specific prompts, multiple expert avatars with distinct preferences are created. Each avatar produces a 5-point Likert score for every therapy chunk; the final automated score is the median-of-five, with standard deviation computed across avatars.

2. Human Stratified Evaluation: stratified sampling based on standard-deviation quantiles of inter-avatar disagreement, yielding low, medium, and high discordance strata. Human reviewers re-score a pre-specified fraction within each stratum; if Cohen's k < 0.8, the entire stratum is re-sampled (max 3 rounds). Iteration terminates when k > 0.8 or 95 % CI width < 5 % of the stratum mean. The full workflow is shown in Figure 4.

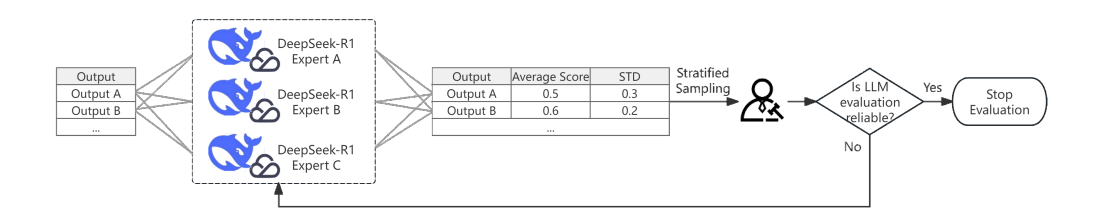


Figure 4: Hierarchical Evaluation Pipeline

#### 2.6. Generalization Evaluation

To validate KRAL's generalization capability, evaluation experiments were conducted on two held-out datasets: MedQA and PUMCH Antimicrobial. MedQA tests factual antimicrobial knowledge; PUMCH Antimicrobial tests multi-step clinical reasoning. Accuracy@1 (MedQA) and Pass@1 (PUMCH) were pre-specified primary end-points; 95 % CIs are Clopper-Pearson; multiple-comparison correction (Holm–Bonferroni) applied across 3 groups (RAG, SFT, KRAL). Student model architecture: DeepSeek-R1-Distill-Qwen-32B (32 B params); identical base model for RAG, SFT and KRAL to ensure fair comparison. RAG and SFT methods were selected as control approaches for knowledge augmentation and reasoning enhancement, respectively. Hyper-parameters for RAG (Table 2), SFT (Table 3) and inference (Table 4) were grid-searched on 20 % held-out development split; best median dev score was locked before final test evaluation.

#### 2.7. Ablation Study

To validate the effectiveness of the proposed algorithmic optimizations, we quantify the marginal contribution of each component via ablation experiments on the PUMCH Antimicrobial benchmark. Primary end-point: mean token-level reward averaged over three random seeds (42, 123, 2024). Four

Table 3: RAG Setting

Key	Value	Key	Value
Chunk size Chunk overlap	256 tokens 32 tokens	Dense weight Sparse weight	0.4 0.2
Embedding model	BAAI/BGE-m3	Colbert weight	0.4
Search type	Hybrid search	Colbert dimension	1024
topk	3	Filter threshold	0.3

Table 4: Model Inference Setting

Key	Value	Key	Value
GPUs	4*NVIDIA L20	Temperature	0.2
Inference Server	m vllm	Think mode	true
Tensor Parallelism	4	Max tokens	4096
GPU utilization	60%	Top p	0.01
Max model length	20480	n	1

factors were systematically ablated as in Table 5. Experiments were performed on the PUMCH benchmark with training parameters consistent with Table 2 in the GRPO Training Process, utilizing computational resources from 8 \* NVIDIA L20 GPUs.

# 3. Results

KRAL simultaneously boosts antimicrobial knowledge (MedQA Accuracy@1 +1.8 % vs SFT, +3.6 % vs RAG) and clinical reasoning (PUMCH Pass@1 +27 % vs SFT, +27.2 % vs RAG) while cutting compute cost by  $8\times$  and VRAM by  $100\times$ , details are as follows.

# 3.1. Knowledge Retrieval Efficiency

We benchmark against BAAI's official algorithm(FlagEmbedding) on 200 randomly sampled training queries using single NVIDIA L20[48 GB], batch

Table 5: Ablation Study Setting

Factor	Description	Ablated Setting
Clip-Higher	asymmetric advantage clipping	$[+0.4, -0.2] \rightarrow \pm 0.2$
Reward Smoothing	custom EMR-aware reward	$\begin{array}{c} \text{hybrid similarity} \rightarrow \\ \text{precise match} \end{array}$
Sub-word Jaccard	token-level match	$\begin{array}{c} \text{sub-word} \rightarrow \\ \text{word-level} \end{array}$
Repetition Penalty	surface-form penalty	$\lambda = 0.1 \rightarrow 0$

size = 1, warm cache. After hybrid searching, re-ranking and tensor parallelism optimization, mean latency dropped from 1.415 s  $\rightarrow$  0.873 s (paired t-test, p < 0.001), a 38 % reduction (Table 6).

Table 6: Needle-in-a-Haystack (NiH) Test

	Dense Retrieval	Hybrid Retrieval
Top@1	71.2%	76.6%
Top@3	85.9%	87.9%
Top@5	88.9%	90.7%

Table 7: Query Latency Test

BAAI Official Algorithm[29]	Our Implementation
1.415s	0.873s

# 3.2. Supervised Fine-Tuning & GRPO Training Results

SFT achieved optimal validation accuracy of  $0.792 \pm 0.02(2800 \text{ steps})$ , early stopping). GRPO reached a peak validation reward of  $0.77 \pm 0.01$  after 12k training steps. Learning curves are smoothed with Exponential Moving Average ( $\beta = 0.8$ ) and shown in Figure 5 (SFT) and Figure 6 (GRPO).

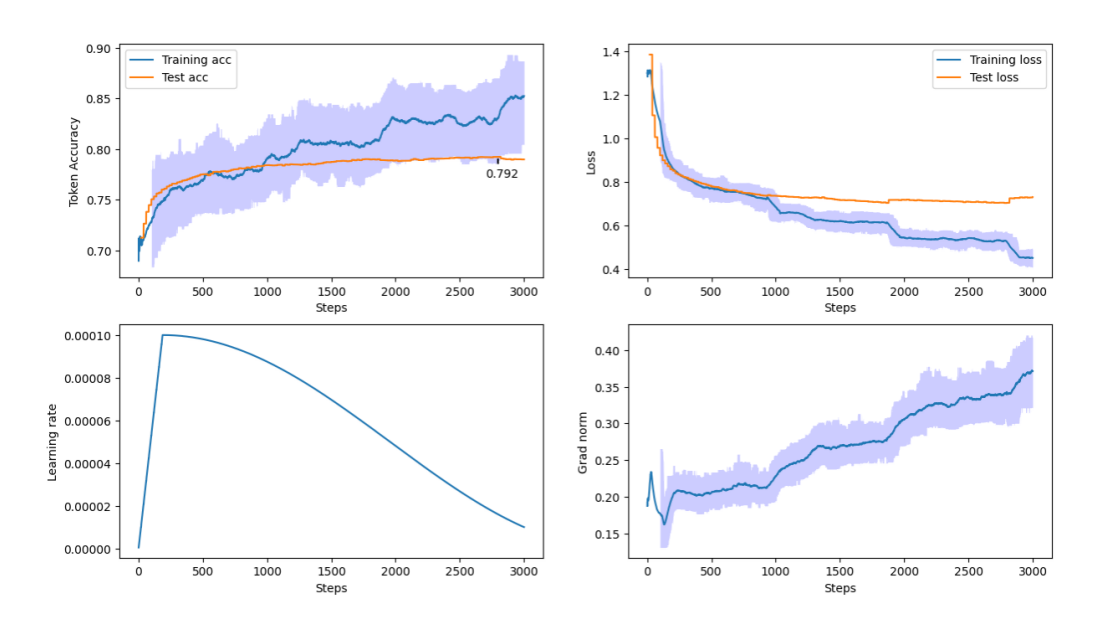


Figure 5: SFT Process

# 3.3. Hardware Efficiency

Combined optimisations (LoRA-r16, FP8, ZeRO-3, CPU-offload, C.R.M) yield:

$$FLOPs_{KRAL} = 0.25_{LoRA} \times 0.5_{C.R.M} = 0.125$$
 (8× reduction)

 $VRAM_{KRAL} = 0.33_{LoRA} \times 0.5_{FP8} \times 0.125_{offload} \times 0.5_{C.R.M} \approx 0.0103$  (100× reduction) Taking fine-tuning or RL with a 32B model as an example:

- 1. **Theoretical full fine-tuning**: 384 GB VRAM (64 params + 64 grad + 256 Adam).
- 2. Full RL (PPO): > 1.15 TB VRAM ( $3 \times$  models, at least 16 A100 or H100 GPUs).
- 3. **KRAL**:  $4 \times L20$ -48 GB for SFT,  $8 \times L20$ -48 GB for GRPO (Table 6).

So KRAL can achieve high hardware efficiency on limited resource which enables practical deployment.

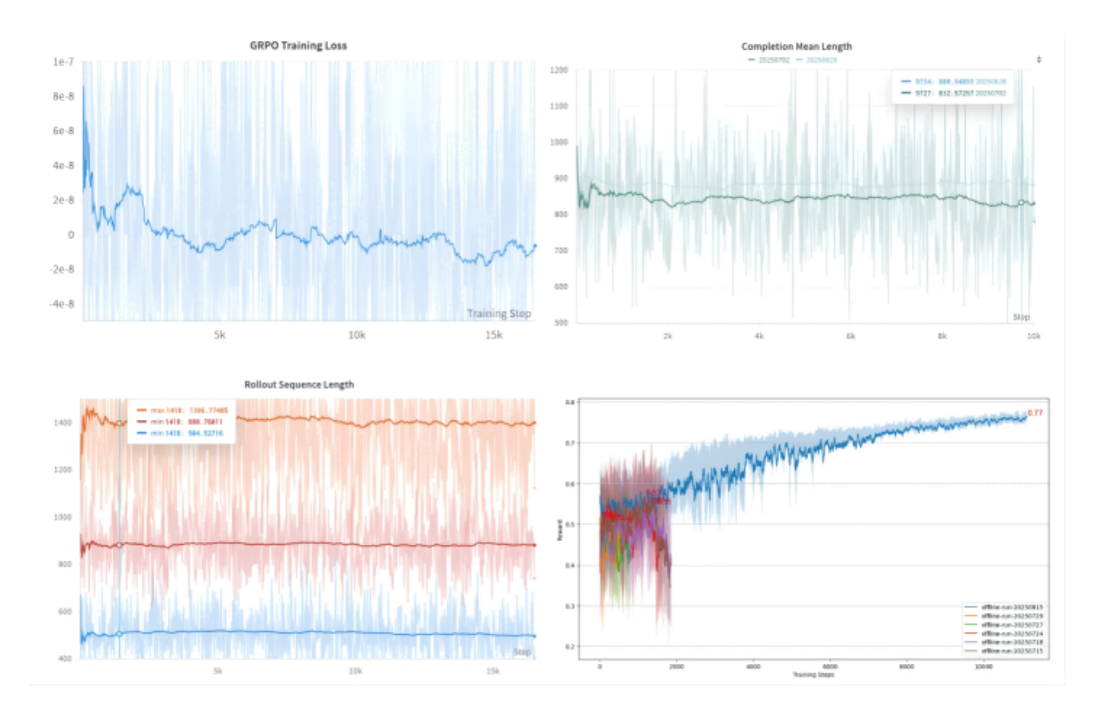


Figure 6: GRPO Training Process

Table 8: Hardware Efficiency before & after optimization

	Before Optimal	$\begin{array}{c} {\bf After} \\ {\bf Optimization} \end{array}$
SFT	8 × A100/H100 (80G) Expensive (\$72k -	4 × RTX4090/L20 (24–48G) Cheap (\$8k–\$16k)
RL	\$240k) >16 × A100/H100 (80G)	$8 \times L20 (48G)$
	Expensive (\$14k-\$48k)	Cheap (\$32k)

# 3.4. Generalization Evaluation

# 3.4.1. External open-source benchmark MedQA

Evaluation results demonstrate that the KRAL method achieves a +1.8% accuracy improvement over SFT and a +3.6% improvement over RAG with

statistical significance mark '\*' in Figure 7. This validates that the KRAL method can effectively achieve knowledge augmentation even on external test sets.

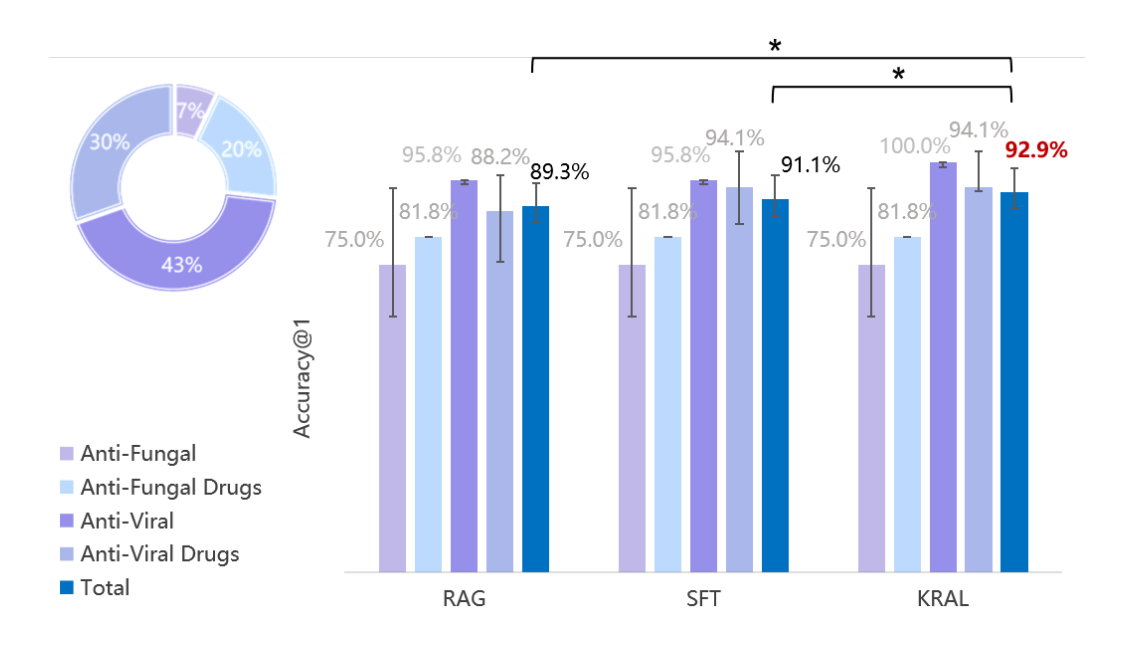


Figure 7: MedQA distribution & evaluation result

## 3.4.2. External proprietary PUMCH benchmark

Considering the unstructured nature of the data, the Pass@1 metric was used to evaluate whether treatment plan keywords were accurately identified. Evaluation was conducted on approximately 100 data points. Results demonstrate that KRAL significantly outperforms RAG and SFT across all three subtasks marked by '\*' in Figure 8. Overall Pass@1 improved by +27% compared to SFT and +27.2% compared to RAG, validating the effectiveness of enhanced medical reasoning capabilities in real clinical scenarios.

# 3.4.3. Comprehensive Comparison

The comprehensive comparison across both test datasets, incorporating additional dimensions such as hardware utilization and data security, is presented in Fig. 9. Here, K.A. denotes Knowledge Augmentation, and R.A. denotes Reasoning Augmentation. Their respective values are derived from Accuracy@1 \* 100 on the MedQA evaluation set and Pass@1 \* 100 on the

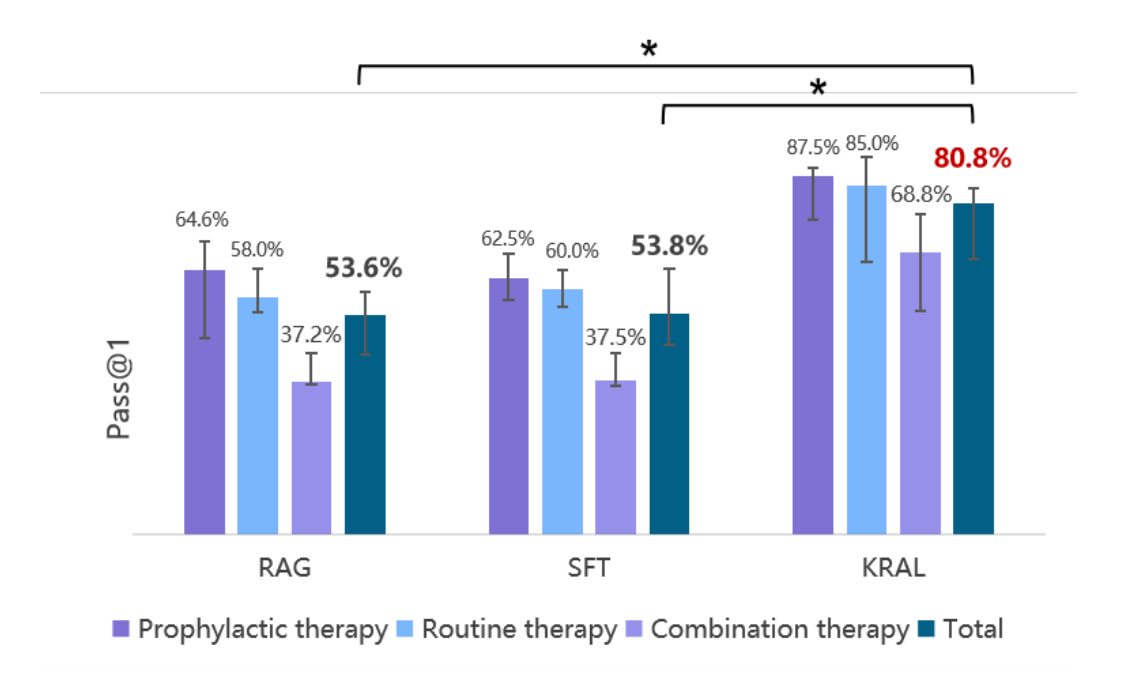


Figure 8: Results on PUMCH benchmark

PUMCH Antimicrobial evaluation set. Training Cost represents the combined cost of GPU resource allocation and training data annotation. Since RAG does not involve training, it is excluded from comparison, with SFT training cost serving as the baseline. Analysis of actual runtime testing and Table 4 indicates that training the 32B student model KRAL requires at least 8 L20 GPUs, while traditional full-parameter SFT demands at least 8 A100 GPUs. LoRA-efficient parameter tuning SFT requires at least 4 L20 GPUs. Training data comprises approximately 10K entries, with annotation costs estimated at \$2 per medical record (including diagnostic reasoning chain). Teacher model API pricing per million tokens is negligible. Hardware configuration and annotation cost comparisons are as follows:

- 1. Full-parameter SFT: > \$72,000 + \$20,000 = \$92,000
- 2. **LoRA SFT**: \$16,000 + (\$2 \* 10,000) = \$36,000
- 3. **KRAL**: \$32,000 + (\$2 \* 2,000) = \$36,000

In the short term, KRAL costs are comparable to efficient SFT; in the long term, as the labeling cost advantage (1:5 ratio) accumulates, hardware costs are gradually amortized, ultimately requiring only about 20% of SFT's ex-

penditure. Compared to traditional SFT, KRAL offers both cost and performance advantages.



Figure 9: Results for K.A., R.A., Training Cost and Data Safety

## 3.5. Ablation Study

Results shown in Figure 11 demonstrate that the optimization proposed in this study enable RL training with better performance and greater stability.

## 4. Discussion

The proposed KRAL paradigm achieves significant performance improvements in clinical antimicrobial treatment decision-making through its dual-enhancement framework for knowledge and reasoning capabilities. Experimental results demonstrate that this framework addresses core bottlenecks in traditional methods—such as medical knowledge gaps, data security, deployment costs, and reasoning limitations—while providing a feasible pathway for deploying LLMs in resource-constrained healthcare settings. From a technological innovation perspective, KRAL's three-stage learning framework (data distillation, agent reinforcement learning, multi-expert evaluation) forms a closed-loop optimization mechanism.



Figure 10: Results of the ablation experiments

During the data distillation phase, a vector knowledge base was constructed from PUMCH clinical guidelines, achieving optimized knowledge retrieval performance. Test results indicate that the proposed Hybrid Retrieval approach reduces processing time by 38% compared to the official BAAI implementation. We developed a heuristic medical data distillation technique, leveraging knowledge chunks to guide LLMs in reverse-generating Q&A training data (answer-to-question generation). Employing a semi-supervised data augmentation strategy, we utilized few-shot prompt engineering to guide large language models in generating similar queries, expanding seed data from 2k to 10k instances and effectively addressing the scarcity of medical annotated data. Faced with massive unstructured clinical data, reasoning teacher model(e.g., DeepSeek-R1) innovatively leverages its reasoning capability to manage and filter raw clinical data, drastically reducing manual data curation costs. With screened data, DeepSeek-R1 employs its explicit

reasoning capability and agentic RAG technique to achieve comprehensive documentation of clinical reasoning chains and guideline references.

During the training phase, we introduced Agentic RL for transfer training in the medical domain. Agentic RL treats the student LLM as a complete agent capable of long-term action, planning, and reflection within dynamic environments. It employs RL for end-to-end optimization of the agent's multi-step decision policy, rather than merely refining the rationality of single responses. Compared to traditional RLHF's single-step decision-making, Agentic RL explicitly extends the decision-making chain, making it highly suitable for complex, multi-round clinical scenarios. These scenarios require iterative knowledge retrieval based on patients' intricate medical histories, conditions, and drug interactions. Simultaneously, online invocation of knowledge retrieval tools during training effectively mitigates hallucinations of critical information—such as medication dosages—even with limited finetuning data. Differences from traditional RL are detailed in Appendix C5. To better adapt to medical tasks, a customized Medical-GRPO algorithm was developed to enhance training stability, with ablation experiments validating its effectiveness. Notably, to overcome hardware efficiency bottlenecks, a combined optimization scheme employing LoRA parameter fine-tuning, FP8 mixed-precision computation, ZeRO-3 parallel strategy, memory offloading, and compressed reward models reduced computational power consumption by 8-fold and memory usage by 100-fold. This enabled SFT training of 32B-parameter models on consumer-grade GPUs and reinforcement learning training on 8 L20 GPUs. The evaluation phase established a hierarchical multi-expert assessment system. By combining preliminary screening using large models with stratified sampling by human experts, this system ensured evaluation accuracy while controlling costs.

Evaluation experiments were conducted across two dimensions: the publicly available MedQA test set and the proprietary PUMCH Antimicrobial QA test set. The MedQA set, a widely used benchmark derived from professional medical examinations, assesses large models' medical question-answering capabilities. The PUMCH set, designed by Peking Union Medical College Hospital experts, utilizes de-identified clinical data. Training and evaluation datasets showed no overlap. Evaluation metrics included Accuracy@1 and Pass@1. Results demonstrate that the KRAL framework achieves a 1.8% higher Accuracy@1 than baseline model (DeepSeek-R1-Distill-Qwen-32B) on MedQA, validating its knowledge enhancement and generalization. On the PUMCH Antimicrobial QA dataset, KRAL achieved an

80.8% Pass@1 rate, significantly outperforming traditional SFT (53.8%) and RAG (53.6%). This demonstrates that distilling reasoning paths and incorporating agentic reinforcement learning substantially improve student models' decision-making performance, especially in complex tasks like comorbidities management and drug resistance risk assessment, validating the reasoning enhancement effectiveness.

Compared to traditional approaches, the core advantages of KRAL include:

- 1. Knowledge Augmentation Traditional SFT impairs general knowledge retention, and excessive samples may even cause performance degradation [30]. KRAL generates answers via heuristic data distillation, leveraging both the knowledge base and the model's pre-trained general knowledge. This approach adapts techniques from SFT with mixed pre-training corpora to minimize general knowledge loss while avoiding the additional training costs associated with dataset expansion.
- 2. Reasoning Augmentation The DeepSeek-R1 technical report demonstrates reinforcement learning's significant role in enhancing model reasoning. Agentic reinforcement learning further integrates chain-of-thought (CoT) techniques, utilizing step-by-step guidance to ensure continued improvement in reasoning abilities. Unlike traditional fine-tuning, research indicates that many "medically fine-tuned" LLMs struggle with general reasoning on untrained medical tasks, particularly in comprehension, text generation, and encoding [31]. In contrast, models trained with agentic reinforcement learning maintain strong generalization on external evaluation datasets.
- 3. Hardware Efficiency While traditional RAG offers low deployment costs, it fails to enhance the model's inherent reasoning capabilities and cannot be directly applied in complex medical scenarios. Traditional SFT incurs substantial computational/storage overhead and data requirements [32]. For complex or long-context tasks, fine-tuning models necessitates extensive labeled data and domain-specific corpora to achieve improvements [30]. KRAL constructs a multidimensional data augmentation system through semi-supervised enhancement and LLM-assisted mining, significantly reducing manual annotation demands and costs. A fivefold data expansion achieves an 80% reduction in annotation expenses. Furthermore, by combining efficient LoRA fine-tuning, FP mixed-precision training, Zero3 model partitioning, and parame-

ter unloading optimization, KRAL substantially reduces computational resource consumption and VRAM usage during training. This enables reinforcement fine-tuning of hundred-billion-parameter models on consumer-grade GPUs.

- 4. **Data Safety** The 100× VRAM reduction permits on-premise deployment within hospital firewalls, eliminating transmission of raw PHI to external APIs and ensuring HIPAA/GDPR compliance by design—an inherent advantage over cloud-based closed-source services (e.g., GPT-5, Gemini).
- 5. Knowledge & Reasoning Scalability Local deployment supports push-button knowledge refreshes via PDF/CSV uploads and hot-swapping of teacher checkpoints (e.g., from DeepSeek-R1 to Med-Gemini). Following updates to either knowledge or the teacher model, the entire process operates automatically, requiring only minimal human intervention for sample verification. Furthermore, the same student model can integrate multiple checkpoints from different iterations into one latest checkpoint, enabling continuous augmentation.

Limitations of this study include: (1) Domain restriction: guidelines cover only antimicrobial therapy; oncology/cardiology generalization performance remains to be proven. (2) Teacher bias: distilled reasoning trajectory inherit any heuristic or cognitive bias present in the teacher model, potentially propagating systematic errors. (3) Sample size: evaluation cohort is modest; multi-centre, longitudinal audits (>10 000 cases) are planned to confirm long-term clinical benefit.

#### 5. Conclusion

This study proposes a Knowledge and Reasoning Augmented Learning (KRAL) paradigm to address four core challenges in applying large models to clinical antimicrobial therapy: medical knowledge bias, data security risks, high deployment costs, and insufficient reasoning capabilities. Through dual-source distillation of vectorized knowledge bases and teacher model reasoning trajectories, combined with an Agentic Reinforcement Learning strategy, KRAL achieves efficient transfer of knowledge and reasoning capabilities while maintaining HIPAA/GDPR compliance via on-premise deployment. External evaluations show superior knowledge retention (MedQA +1.8 % vs SFT) and clinical reasoning (PUMCH Pass@1 +27 % vs SFT) at 20 % of

long-term annotation cost and 100 times less VRAM.Multi-centre trials and extension to oncology/cardiology guidelines will be pursued to confirm generalization performance. This paradigm offers a new approach for low-cost, high-safety application of LLMs in complex clinical decision-making scenarios, potentially accelerating the large-scale implementation of AI in precision medicine.

# 6. Funding

This work was supported by the Beijing Municipal Natural Science Foundation (L222019); CAMS Innovation Fund for Medical Sciences (CIFMS) (2024-I2M- C&T-C-002); National High Level Hospital Clinical Research Funding (2022-PUMCH-B-115&2022-PUMCH-D-005); and National Key R&D Program of China (2024YFF1207104).

# 7. Acknowledgments

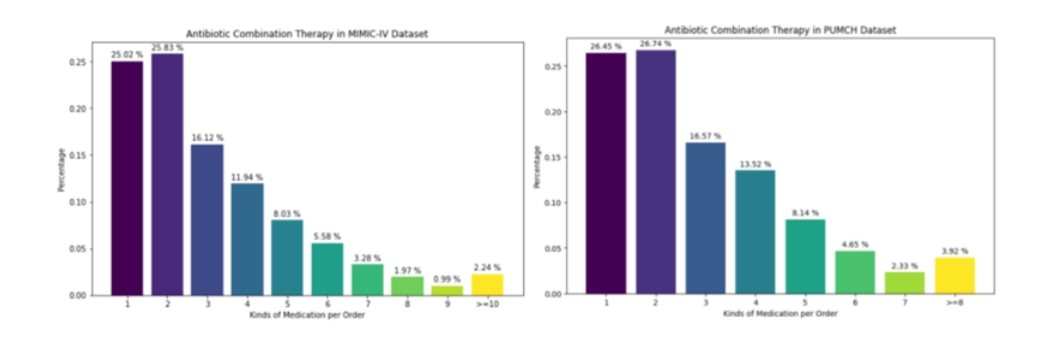
Group authorship: China Critical Care Clinical Trials Group (CCCCTG) and China National Critical Care Quality Control Center Group (China-NCCQC group).

# Appendix A.

Appendix A.1. Time Difference Between Mainstream Model Release Dates and Pre-Training Knowledge Updates, Data Sources [4-8]

Model	Corpus Update Time	Release Date	Gap(month)	Data Source
GPT-4 Technical Report	GPT-4 Turbo (Apr 2024)	12	arXiv:2303.08774	April 2024
GPT-40 System Card	GPT-40 (Oct 2023)	7	OpenAI, May 2024	May 2024
$\begin{array}{c} \text{Qwen2-VL} \\ \text{paper} \end{array}$	$\begin{array}{c} \text{Qwen2-VL (Jun} \\ 2023) \end{array}$	20	arXiv:2409.12191	February 202
DeepSeek-V2 paper	DeepSeek-V2 (Dec 2023)	5	arXiv:2405.04434	May 2024
Claude 3 Model Card	Claude 3 (Aug 2023)	7	Anthropic, March 2024	March 2024

 $Appendix \ A.2. \ MIMIC \ IV \ \& \ Peking \ Union \ Medical \ College \ Hospital \ Inpatient \ Antibiotic \ Usage \ Distribution$ 



Dataset	Inclusion and exclusion	Size
Dataset  MIMIC IV  PUMCH	Inclusion and exclusion  Inpatient Orders & Order Type: Antibiotics Admitted in 2024 with orders including antibiotics, not readmitted, and diagnoses related to "infection, pneumonia, enteritis, typhoid fever, dysentery, tuberculosis, viral encephalitis." Order name contains: "Penem" or "Mycin" or "Cef" or "Floxacin" or "Lover" or "Coxazol" or "Piracilin" or "Tigecycline" or "Tecolaran" or "Capreomycin" or "Metronidazole" or "Polymyxin" or "Amikacin" or "Sulfamethoxazole" or	Size $40687720 \rightarrow 848482$ $3999->710$
	"Linezolid" or Doxycycline or Amoxicillin	

## Appendix B.

Appendix B.1. Knowledge Distillation Q&A pair sample Q&A pair are as follows:

#### Question

"What are the symptoms of childhood chlamydia infection?"

#### Answer

Typical symptoms of chlamydia infection in children primarily include: 1. No fever The infection typically does not cause a fever (unlike bacterial infections). 2. Staccato cough Characterized by short, frequent dry coughs resembling a "machine gun" cough. 3. Persistent cough In older children or adolescents, this may manifest as a cough lasting longer than 2 weeks (requiring differentiation from pertussis or mycoplasma infection). 4. Laboratory Indicators Serum IgM antibody titer >1:8 supports the diagnosis of Chlamydia trachomatis infection. Additional Considerations

- Neonatal infection may occur via vertical transmission from mother to child; maternal history should be considered.
- Differential diagnosis is required from bronchitis caused by respiratory syncytial virus (RSV), parainfluenza virus, human metapneumovirus, etc.
- Confirmation requires PCR testing or pathogen culture; treatment prioritizes macrolide antibiotics (e.g., erythromycin or azithromycin).

# Reasoning content

The user is inquiring about symptoms of childhood chlamydia infection. I need to retrieve relevant information from the provided knowledge base. First, knowledge index 199 indicates that in neonates presenting with afebrile, paroxysmal cough and IgM antibody titer >1:8, Chlamydia trachomatis infection should be considered, with treatment using erythromycin or sulfamethoxazole. The key symptoms here are absence of fever and paroxysmal cough.

Next, knowledge index 192 states that in adolescents and adults with acute bronchitis, Mycoplasma or Chlamydia infections may cause persistent cough lasting over two weeks, typically without fever. Although this pertains to older children and adults, pediatric Chlamydia infections may also present similar symptoms, such as persistent cough.

Additionally, knowledge index 332 addresses neonatal sepsis, primarily bacterial but potentially involving chlamydial infections—particularly Chlamydia trachomatis—in newborns, presenting with afebrile cough.

Synthesizing this information, key symptoms of childhood chlamydia infec-

tion include fever-free, paroxysmal coughing, potentially accompanied by persistent coughing lasting over two weeks, especially in neonates. Laboratory indicators may also show elevated IgM antibodies. Differential diagnosis from other pathogens like mycoplasma or viruses is essential.

Appendix B.2. Reasoning Trajectory Data Sample

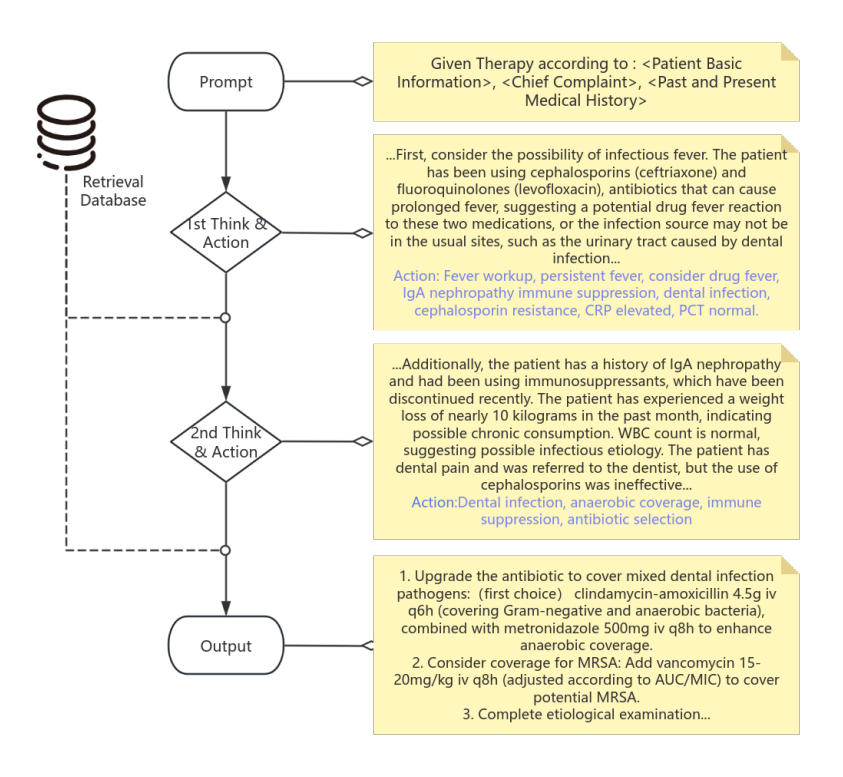


Figure B.11: Antibiotic Usage Distribution

# Appendix C.

Appendix C.1. SFT training dataset sample

For a single row:

Age & gender

Female, 51 years old

Chief complaint

Fever for 12 days

#### Present illness

On 2024-02-23, the patient developed sore throat without apparent cause, followed by afternoon fever with Tmax 39.6°C. She experienced one daily fever peak accompanied by chills and occasional coughing with small amounts of white, mucous-like sputum. She reported mild periodontal pain but denied abdominal pain, diarrhea, frequent urination, or urgency. Self-administered oral cefotiam + throat inflammation powder + traditional Chinese medicine, with minimal symptom relief. Due to excessive sweating after taking Tylenol, the patient took it only once; subsequently, fever resolved spontaneously each day. Consulted local dental department, where periodontal inflammation was suspected. Discontinued aforementioned medications and switched to ciprofloxacin 2 qd. Fever persisted daily without resolution. 03-01 Visit to Tsinghua University Hospital: Blood count: WBC 7.38×10\*9/L, NEUT% 62.5%, EOS% 0.06%, HGB 121g/L, MCV 91.5fl, MCHC 331g/L, PLT 402 \* 10<sup>9</sup>/L Inflammatory markers: hsCRP 131.00 mg/L, SAA 350 mg/L, Influenza A/B antigen (-), Mycoplasma pneumoniae + Chlamydia pneumoniae IgM (-). Chest CT: Three ground-glass nodules measuring approximately 2-4 mm in longest diameter were visible in the apical segment, posterior segment of the right upper lobe, and dorsal segment of the right lower lobe. No increased pulmonary markings bilaterally; no other significant abnormalities noted. Presented to our emergency department for further evaluation.

Past medical history On 2024-02-06, presented with sore throat and fever. Self-tested positive for COVID-19 antigen. Administered oral nirmatrelvir/ritonavir. Temperature normalized after 3 days, with subsequent antigen test turning negative. In 2004, proteinuria detected during a physical examination led to a kidney biopsy confirming IgA nephropathy. Regular monitoring was initiated. In October 2021, due to 24-hour urine protein exceeding 0.5g/day, mycophenolate mofetil dispersible tablets were added at 5g bid  $\rightarrow 0.75$ g qd orally. This medication has since been discontinued. Concurrently, elevated uric acid levels were identified, prompting oral administration of febuxostat, which has also been discontinued. In 2020, ultrasound detected a thyroid nodule; fine-needle aspiration showed no tumor cells. Diagnostic recommendations The patient presented with fever, accompanied by sore throat and toothache. A purulent coating was visible on the posterior pharyngeal wall, suggesting possible pharyngitis or periodontitis. Physical examination revealed tenderness over the left maxillary sinus, making maxillary sinusitis a consideration. Cefuroxime 2g qd was added for infection control. and Metronidazole 1g tid to cover anaerobic bacteria. Fever recurred for 2-3 days

with concomitant cough and rhinorrhea. Peripheral blood culture yielded no definitive pathogens. Symptoms gradually resolved, with fever gradually subsiding to normal levels. Cefuroxime and Metronidazole were discontinued, replaced with Levofloxacin tablets 0.5g qd. Temperature remained consistently normal.

Appendix C.2. Unstructured evaluation dataset sample

For a single row:

#### Question

Patient, male, 65 years old, admitted for "recurrent reducible mass in right inguinal region for 2 years," diagnosed with "right inguinal hernia," scheduled for "laparoscopic tension-free inguinal hernia repair." No history of drug allergies or other underlying conditions. How should prophylactic antibiotics be administered?

# Raw knowledge

{'chunk-id': c124, 'content': 'Clean surgeries (such as inguinal hernia repair) typically do not require routine prophylactic medication. However, for hernia repairs involving synthetic mesh implants, prophylactic antibiotics are recommended. Recommended regimen: A single intravenous dose of cefazolin 1-2g administered 30 minutes preoperatively. Alternatively, a single intravenous dose of ampicillin-sulbactam 3g, clindamycin 900mg, or vancomycin 1g may be administered. No postoperative boost is required.', 'page-no': 124}

#### Answer

"Cefazolin 1-2g" or "Amoxicillin-Sulbactam 3g" or "Clindamycin 900mg" or "Vancomycin 1g"

Appendix C.3. MedQA data sample

A 27-year-old male presents to urgent care complaining of pain with urination. He reports that the pain started 3 days ago. He has never experienced these symptoms before. He denies gross hematuria or pelvic pain. He is sexually active with his girlfriend, and they consistently use condons. When asked about recent travel, he admits to recently returning from a boys' trip' in Cancum where he had improtected sex! I night with a girl he met at a bar. The patients medical history includes type! diabetes that is controlled with an insulin pump. His mother has rheumatoid arthritis. The patients temperature is 99 F (37.2 C), blood pressure is 112/74 mmHg, and pulse is 81/min. On physical examination, there are no levisions of the penis or other body rashes. No contovertebral tenderness is appreciated. A virinely size reveals no blood, glooce, ketones, or proteins but is positive for leukocyte esterates. A urine microscopic evaluation shows a moderate number of white blood cells but no casts or crystalls. A urine culture is negative. Which of the following is the most likely cause for the patient's symptoms?
A: Chlamydia trachomatis, B: Systemic lupus erythematosus, C: Mycobacterium tuberculosis, D: Treponema pallidum
At least one-third of male patients with C. trachomatis urethral infection have no evident signs or symptoms of urethritis Such patients generally have pyuria, a positive leukocyte esterase test,
A 57-year-old man presents to his primary care physician with a 2-month history of right upper and lower extremity weakness. He noticed the weakness when he started falling far more frequently while running errands. Since then, he has had increasing difficulty with walking and lifting objects. His past medical history is significant only for well-controlled hypertension, but he says that some members of his family have had musculoskeletal problems. His right upper extremity shows forearm atrophy and depressed reflexes while his right lower extremity is hypertonic with a positive Babinski sign. Which of the following is most likely associated with the cause of this patients symptoms?
A: HLA-B8 haplotype, B: HLA-DR2 haplotype, C: Mutation in SOD1, D: Mutation in SMN1, E: Viral infection
1. The manifestations of ALS insidiously developing asymmetric weakness, usually first evident distally in one of the limbs.     2 hyperactivity of the muscle-stretch reflexes (tendon jerks) and, often, spastic resistance to passive movements     3. Familial ALS (FALS) clinically indistinguishable from sporadic ALS Genetic studies have identified mutations in multiple genes, including cytosolic enzyme SOD1

Appendix C.4. PUMCH Antimicrobial Sample

For a single row:

## Query

Patient, female, 58 years old, has been hospitalized multiple times for "complicated urinary tract infection." Current urine culture results: ESBL-producing Escherichia coli resistant to ceftriaxone and fluoroquinolones, with susceptibility only to carbapenems and amikacin. How should the treatment regimen be selected?

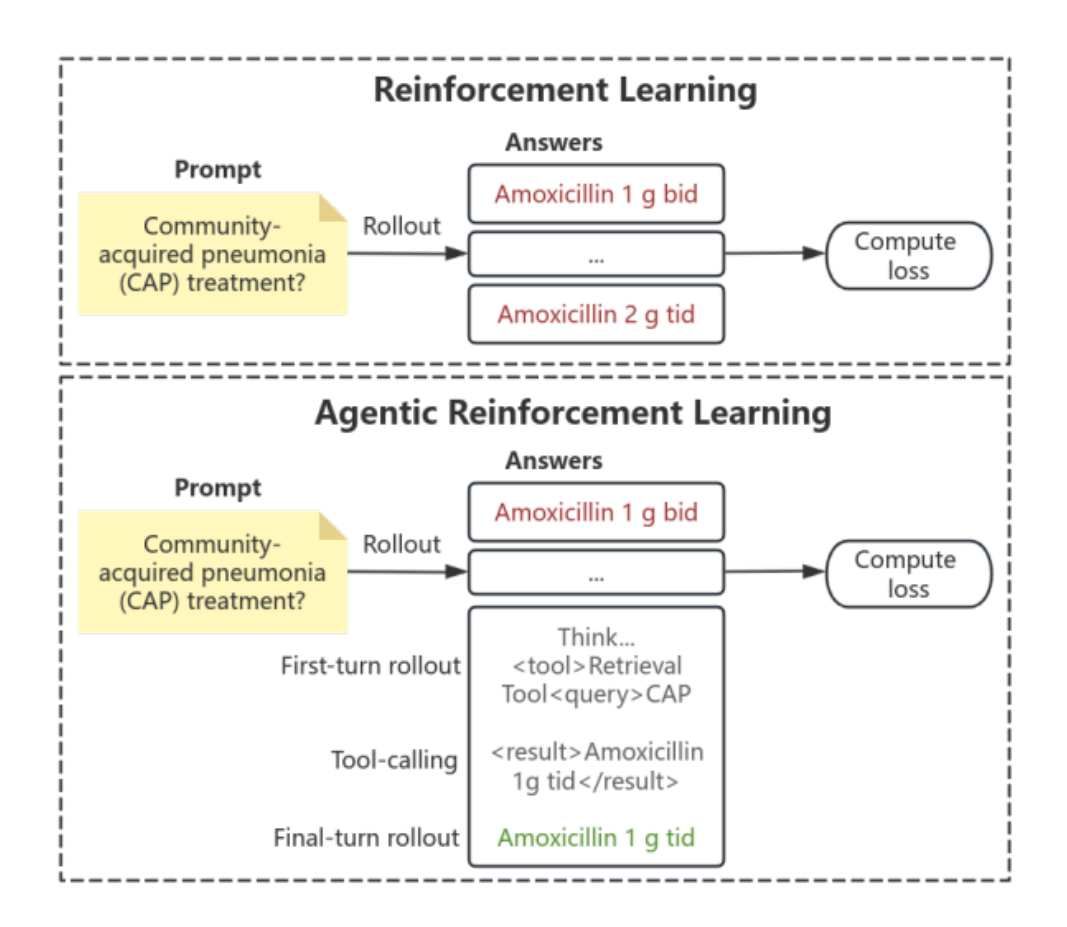
## Therapy

For severe infections caused by ESBL-producing Enterobacteriaceae (e.g., pyelonephritis, bacteremia), guidelines recommend carbapenems as standard therapy. Options: IV infusion of Ertapenem 1g q24h or Meropenem 1g q8h or Imipenem-Cilastatin 500mg q6h.

## **Keywords**

"Ertapenem," "Meropenem," "Imipenem-Cilastatin"

Appendix C.5. Agentic Reinforcement Learning vs. Reinforcement Learning



#### References

- [1] T. Brown, et al., Language models are few-shot learners, OpenAI Blog (2020).
- [2] T. Hulsen, Explainable artificial intelligence (xai): Concepts and challenges in healthcare, AI 4 (2023) 652–666.
- [3] Y. Li, Y. Li, M. Wei, et al., Innovation and challenges of artificial intelligence technology in personalized healthcare, Sci Rep 14 (2024) 18994.

- [4] L. Celi, J. Cellini, M.-L. Charpignon, et al., Sources of bias in artificial intelligence that perpetuate healthcare disparities—a global review, PLoS Digit. Health 1 (2022) e0000022.
- [5] OpenAI, Gpt-4 technical report, Tech. Rep. arXiv:2303.08774 (2023).
- [6] OpenAI, Gpt-4o system card (May 2024).
- [7] J. Bai, et al., Qwen2-vl: Enhancing vision-language model's perception of the world at any resolution, arXiv preprint (arXiv:2409.12191) (September 2024).
- [8] DeepSeek-AI, Deepseek-v2: A strong, economical, and efficient mixture-of-experts language model, Tech. Rep. arXiv:2405.04434 (May 2024).
- [9] Anthropic, Claude 3 model card and system report, Tech. rep. (March 2024).
- [10] C. Wang, J. Zhang, N. Lassi, X. Zhang, Privacy protection in using artificial intelligence for healthcare: Chinese regulation in comparative perspective, Healthcare 10 (2022) 1878.
- [11] B. Murdoch, Privacy and artificial intelligence: challenges for protecting health information in a new era, BMC Med Ethics 22 (2021) 122.
- [12] H. Zhang, J. Chen, M. Wang, H. Li, X. Zhou, Privacy leakage in large language models: A comprehensive survey, arXiv preprint (2023).
- [13] E. Ullah, A. Parwani, M. Baig, et al., Challenges and barriers of using large language models (llm) such as chatgpt for diagnostic medicine with a focus on digital pathology—a recent scoping review, Diagn Pathol 19 (2024) 43.
- [14] M. DJ, C. MP, P. E, et al., Artificial intelligence in low- and middle-income countries: Innovating global health radiology, Radiology 297 (3) (2020) 513–520.
- [15] F. J, G. L, C. VM, M.-I. C, L. K, Federated learning in low-resource settings: A chest imaging study in africa — challenges and lessons learned, arXiv (2025).

- [16] W. D, H. H, N. A, P. A, Deep learning and its application for healthcare delivery in low and middle income countries, Frontiers in Artificial Intelligence 4 (2021) 553987.
- [17] Y. Huang, K. Tang, M. Chen, et al., A comprehensive survey on evaluating large language model applications in the medical industry, arXiv preprint (2024).
- [18] K. Singhal, S. Azizi, T. Tu, et al., Large language models encode clinical knowledge, Nature 620 (2023) 172–180.
- [19] Z. Guo, R. Jin, C. Liu, et al., Evaluating large language models: A comprehensive survey, arXiv preprint (2023).
- [20] S. Yao, J. Zhao, D. Yu, et al., React: Synergizing reasoning and acting in language models, in: International Conference on Learning Representations (ICLR), 2023.
- [21] D. Guo, D. Yang, H. Zhang, et al., Deepseek-r1 incentivizes reasoning in llms through reinforcement learning, Nature 645 (2025) 633–638.
- [22] Z. Shao, P. Wang, Q. Zhu, et al., Deepseekmath: Pushing the limits of mathematical reasoning in open language models (2024).
- [23] E. Hu, Y. Shen, P. Wallis, et al., Lora: Low-rank adaptation of large language models (2021).
- [24] S. Rajbhandari, J. Rasley, O. Ruwase, Y. He, Zero: Memory optimizations toward training trillion parameter models (2020).
- [25] J. Ren, S. Rajbhandari, R. Aminabadi, et al., Zero-offload: Democratizing billion-scale model training (2021).
- [26] B. M., K. R., M. H., et al., Communication-efficient jaccard similarity for high-performance distributed genome comparisons, in: 2020 IEEE International Parallel and Distributed Processing Symposium (IPDPS), 2020, pp. 1122–1132.
- [27] B. Biswas, R. Ramnath, Efficient and interpretable information retrieval for product question answering with heterogeneous data (2024).

- [28] O. Khattab, M. Zaharia, Colbert: Efficient and effective passage search via contextualized late interaction over bert (2020).
- [29] C. J, X. S, Z. P, et al., Bge m3-embedding: Multi-lingual, multi-functionality, multi-granularity text embeddings through self-knowledge distillation (2023).
- [30] Q. Yang, R. Wang, J. Chen, R. Su, T. Tan, Fine-tuning medical language models for enhanced long-contextual understanding and domain expertise (2024).
- [31] F. Dorfner, A. Dada, F. Busch, et al., Biomedical large language models seem not to be superior to generalist models on unseen medical data (2024).
- [32] R. Tinn, H. Cheng, Y. Gu, et al., Fine-tuning large neural language models for biomedical natural language processing, Patterns (New York, N.Y.) 4 (4) (2023) 100729.